INTERACTION OF LASER RADIATION WITH MATTER. LASER PLASMA

PACS numbers: 41.50.+h; 52.50.Jm; 52.40.Nk
DOI: 10.1070/QE2000v030n06ABEH001757

Hard x-ray radiation yield from a dense plasma as a function of the wavelength of the heating ultrashort laser pulse

A Varanavicius, T V Vlasov, R V Volkov, S A Gavrilov, V M Gordienko, A Dubetis, E Zeromskis, A Piskarskas, A B Savel'ev, G Tamosauskas

Abstract. The effect of intensity, length, and wavelength of an ultrashort laser pulse on the formation of a hot electron component in a dense laser-produced plasma was first investigated in a single experiment. For a pulse length of 1 ps (or 200 fs, but with an energy contrast ratio of ~ 20), it was shown that the principal mechanism of generation of hot electrons is the resonance absorption of laser radiation and that the temperature of hot electrons depends on the laser pulse intensity I and the wavelength λ as $T_h \sim (I\lambda^2)^{1/3}$. The homogenisation of the nanostructures of porous silicon due to a poor contrast ratio or a long duration (1 ps) of the laser pulse lowers the yield of hard x-ray radiation compared to the case of high-contrast 200-fs pulses.

1. Introduction

A plasma produced on the target surface by the superstrong light field of an ultrashort laser pulse is a unique source of high-power incoherent x-ray radiation in a broad wavelength range [1]. The soft x-ray radiation in this plasma is formed by the thermal electron component whose temperature depends only slightly on intensity and does not exceed 1 keV. The hard x-ray radiation (with photon energies above 2 keV), on the contrary, is associated with the formation of the so-called hot electron component whose 'temperature' rises steeply with the intensity of the heating laser pulse.

From the standpoint of applications, employing the radiation of 'moderate' intensity of the order of $10^{15} - 10^{17}$ W cm^{-2}, which ensures efficient production of x-ray radiation in the 2 – 20 keV range [2], holds the greatest promise. This interaction mode can be realised using relatively simple and inexpensive table-top laser systems on sapphire, forsterite, neodymium glass, etc. Note that the advancement of laser technology now allows us to attain intensities of 10^{20} W cm^{-2} and over [3], which correspond to hot-electron temperatures above 1 MeV [4].

The efficiency of the generation of hard x-ray radiation can be increased with the use of nanostructured targets [1, 2], in particular, targets of high-porosity silicon. The targets of this type are characterised not only by an augmented total energy of the hot electron component but also by its higher temperature.

To date, a number of experiments have been carried out to measure the efficiency of generation of hard x-ray radiation and, in particular, the generation efficiency in relation to the laser pulse intensity and wavelength [1, 2, 5 – 9]. The results of these experiments provide important information on the prevailing mechanisms of hot-electron production. However, the measurements have been performed so far with the use of different laser radiation sources, employing various diagnostic equipment, and under different experimental conditions.

The following two goals were pursued in this work. One was to investigate, in a single experiment, the dependences of the hard x-ray yield and the temperature of hot electrons in the plasma on the wavelength of an ultrashort laser pulse. The other was to study the effect of laser pulse length and contrast ratio on the efficiency of generation of hard x-ray radiation in high-porosity silicon to provide a physical interpretation of the previously obtained results [1, 2, 5, 6].

2. Experimental setup

The source of laser radiation was a TWINKLE system (Light Conversion Co., Lithuania). This setup provides the unique possibility of obtaining radiation with an intensity of $\sim 10^{16}$ W cm^{-2} at several wavelengths, the laser pulse lengths and the contrast ratios being approximately the same.

The TWINKLE laser system is an actively Q-switched neodymium glass laser with a negative feedback. In combination with chirped-pulse amplification, this allows the formation of picosecond laser pulses at a wavelength of 1055 nm with an output energy of several millijoules and a high stability of the pulse energy and length. Second- and third-harmonic generators allow picosecond pulses to be also obtained at wavelengths $\lambda = 527$ and 351 nm. Employing a compressor at the second harmonic wavelength affords additional capabilities, allowing 200-fs pulses to be formed at $\lambda = 527$ nm.

The TWINKLE system is shown in Fig. 1. It comprises a master oscillator (1), a regenerative amplifier (2), a stretcher (3), a compressor (4), and a harmonic generator (5). Both

A Varanavicius, A Dubetis, E Zeromskis, A Piskarskas, G Tamosauskas Physics Department, Vilnius University, Sauletiko alley 9, Build. 3, LT-2040 Vilnius, Lithuania;
T V Vlasov, V M Gordienko, A B Savel'ev Physics Department, M V Lomo-nosov Moscow State University, Vorob'evy gory, 119899 Moscow, Russia;
R V Volkov International Educational and Scientific Laser Centre, M V Lomonosov Moscow State University, Vorob'evy gory, 119899 Moscow, Russia;
S A Gavrilov Moscow State Institute of Electronic Engineering (Technical University), 103498 Moscow, Russia

Received 30 December 1999
Kvantovaya Elektronika **30** (6) 523 – 528 (2000)
Translated by E N Ragozin, edited by M N Sapozhnikov

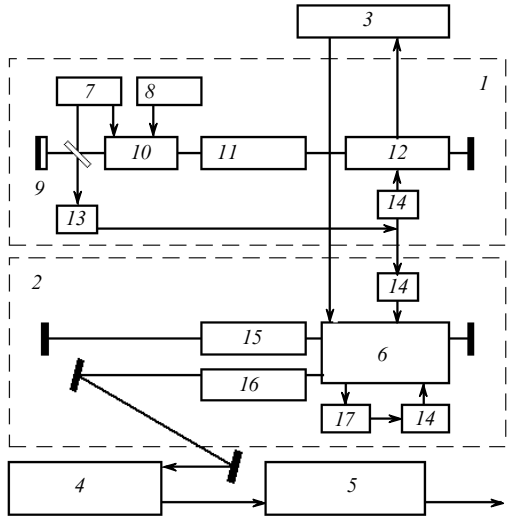

Figure 1. Schematic of the TWINKLE laser system: (1) master oscillator; (2) regenerative amplifier; (3) stretcher; (4) compressor; (5) harmonic generators; (6) device for input and output of single pulses; (7) optical feedback; (8) frequency generator; (9) unit for passive mode locking; (10) electrooptical modulator; (11) amplifying rods; (12) single-pulse extraction device; (13) meter; (14) fast electronic switches; (15) amplifying rods; (16) device for augmenting the contrast ratio; (17) energy meter.

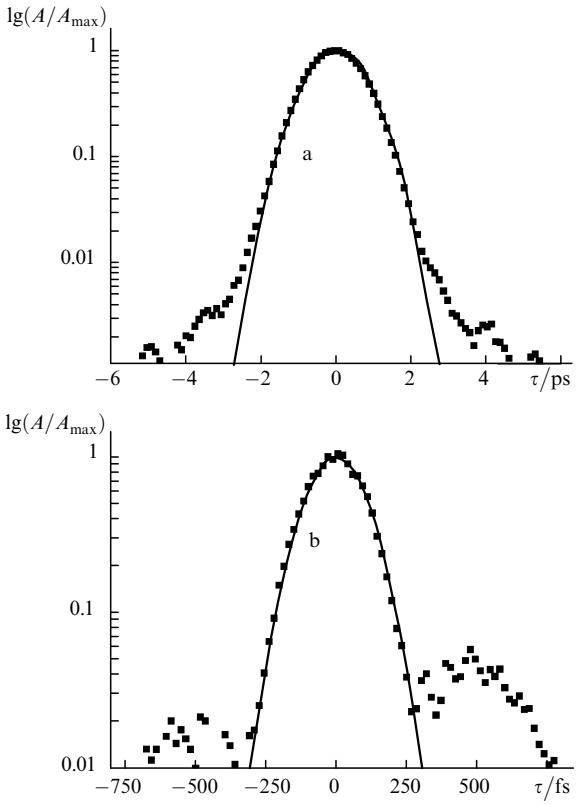

Figure 2. Autocorrelation functions A of the second order for a pulse at the fundamental frequency ($\lambda = 1055$ nm) (a) and of the third order for a second-harmonic pulse ($\lambda = 527$ nm) after the compressor (τ is the delay time; positive delay times correspond to the leading edge of the pulse) (b). The solid lines represent approximations by the Gaussian function. The pulse lengths estimated from the approximations are 1.2 ± 0.1 ps for $\lambda = 1055$ nm and 170 ± 10 fs for $\lambda = 527$ nm.

the master oscillator and the regenerative amplifier consists of two active elements of phosphate glass and $\lambda/2$ plates with a compensation for the thermal lens, which permits stable system operation at a pulse repetition rate up to 10 Hz.

Active-passive mode locking was accomplished by employing a dye cell and a Q-switching with the aid of a Pockels cell. The same cell is used to couple the radiation out of the master oscillator and to form the seed for the regenerative amplifier. The stretcher (3) and the compressor (4) employ gold-coated 1800 line mm^{-1} gratings with reflectivities higher than 95%. The entire system is thermally stabilised to ensure prompt attainment of the operating mode and a long-term stability of the output parameters.

The radiation power in the master oscillator is kept low to guard against self-modulation of the pulse. A single pulse is extracted from the master oscillator (1) with the aid of the Pockels cell and enters the stretcher (3), which increases the pulse length up to 300 ps. The pulse builds up to 15 mJ in the regenerative amplifier (2) with a slight narrowing of its spectrum and negligible self-modulation. The amplified single pulse is extracted using the Pockels cell (6) and arrives at the two-pass compressor (4), where it shortens to 1 – 1.3 ps with energy losses no greater than 35%. Therefore, the output energy of a single laser pulse at $\lambda = 1055$ nm amounts to 10 mJ for a pulse length of 1 ps. The second-order autocorrelation function of the output fundamental-frequency pulse is shown in Fig. 2a.

The output radiation can be converted to other spectral ranges without an increase in pulse length (or with its reduction) and with a high energy efficiency. One version involves second-harmonic generation achieved by employing type-I phase matching in a 12-mm-long KDP crystal with an energy conversion efficiency of 60%. The second version involves third-harmonic generation realised by employing type-II phase matching in a KDP crystal 3 mm long. The energy of $\lambda = 351$ nm pulses amounts to 2.5 mJ, and the pulse lengths are approximately equal to that of the second-harmonic pulses.

The third version provides the radiation conversion to the second harmonic with a simultaneous pulse shortening [10, 11]. The arrangement consists of two KDP crystals of length 15 and 20 mm; the conversion takes place by employing type-II phase matching in both crystals. This compressor provides a fivefold pulse compression with an energy efficiency of conversion to the second harmonic up to 25%. The third-order correlation function for these pulses is shown in Fig. 2b. In addition to the main 200-fs pulse, a broad pedestal 1 ps long with an amplitude of about 5% of the main pulse amplitude is observed.

A precision imaging system equipped with a CCD camera was employed to measure the focal spot diameter D for different wavelengths in the equivalent focal plane. These measurements revealed that the TWINKLE system permits attaining intensities of $\sim 10^{16}$ W cm^{-2} in different spectral regions. The parameters of the laser pulses used in our experiments are listed in Table 1.

The experimental setup for measuring the hard x-ray yield from a laser-produced plasma is shown in Fig. 3. The interaction of a laser pulse with a target was realised at a residual pressure of 10^{-2} Torr in a vacuum chamber (3). The p-polarised radiation was focused on a target (4) with a lens (5) ($f/d = 10$, f is the focal length, d is the beam diameter at the lens, the angle of radiation incidence on the target is 55°). The vacuum chamber was displaced during experi-

Table 1. Parameters of the TWINKLE laser system.

λ / nm	τ_1 / ps	D / μm	W_{max} / mJ	I_{max} / 10^{16} W cm^{-2}	K / 10^5
1055	1	11.7	10	1	5
527	1	6.6	6	1.8	> 5
351	1	5	2.5	1.3	> 5
527	0.2	6.6	2.5	3.7	< 0.0002

Note: λ is the wavelength; τ_1 is the pulse length; D is the focal spot diameter at half maximum $I/2$; W_{max} is the maximum energy of the laser pulse; I_{max} is the maximum intensity of the laser pulse; and K is the energy contrast ratio of the pulse.

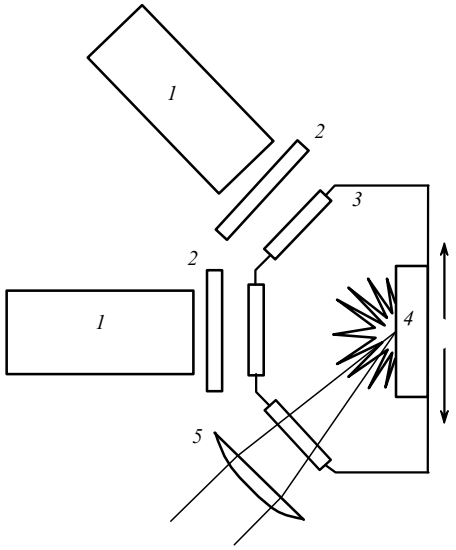

Figure 3. Layout of the experimental setup for measuring the hard x-ray yield from a laser-produced plasma:
(1) x-ray detectors; (2) replaceable filters; (3) vacuum chamber; (4) target; (5) focusing lens.

ments to ensure irradiation of previously unexposed por-tions of the target.

The hard x-ray plasma radiation was recorded with detectors (1) composed of a NaI(Tl) scintillator and a FEU-119 photomultiplier. To measure the hard x-ray yield from the plasma, a prior detector calibration was accomplished using a monochromatic x-ray radiation source (Cu K_α, $E = 8$ keV). The detector response was linear in the x-ray energy range between 3 and 30 keV, which makes the main contribution to the x-ray plasma radiation upon the laser irradiation mode under study. Replaceable combined filters (2) permitted measurements to be made in different x-ray spectral ranges. Fig. 4 shows the transmission coefficients of the filters employed, with account taken for the absorption in the air as functions of the x-ray photon energy.

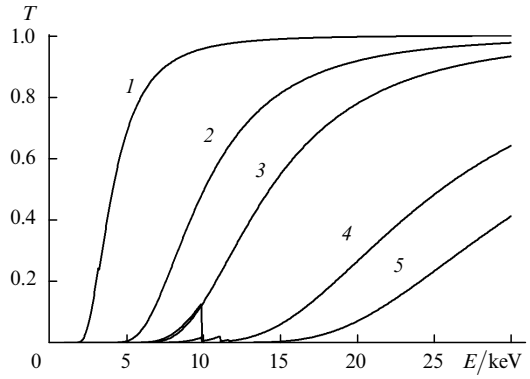

Figure 4. Transmittance T as a function of the x-ray photon energy E for a beryllium filter 200 μm in thickness (1) and the filter combinations Be (200 μm) + Al (100 μm) (2), Be (200 μm) + Al (300 μm) (3), Be (200 μm) + Ta (13 μm) (4), and Be (200 μm) + Ta (26 μm) (5).

3. Effect of laser pulse intensity, contrast ratio, and length on the hard x-ray radiation yield from the plasma

We measured the hard x-ray radiation yield Y from the plasma as a function of the laser radiation intensity I for crystal and high-porosity (porosity of $\sim 70\%$) silicon samples. A 200-μm-thick beryllium filter and this filter in combination with a 100-μm-thick aluminium filter were used (see Fig. 4). The measurements were made invoking the entire set of wavelengths and lengths of the heating laser pulse (see Table 1). The results of measurements are collected in Table 2 and partly shown in Fig. 5.

Consider the results for $\lambda = 0.527$ μm more closely, because in this case, it was possible to vary not only the sample type and the spectral measurement range, but the laser pulse length as well. Fig. 5 shows the hard x-ray radiation yield from the plasma as a function of the laser pulse intensity for the samples of crystal silicon. In the $E > 2.5$ keV energy range, approximating the experimental curve by a power function gives the $Y \sim I^{1.9\pm0.1}$ dependence for crystal silicon and the $Y \sim I^{2.0\pm0.1}$ dependence for porous silicon. In the $E > 6.2$ keV energy range, $Y \sim I^{2.3\pm0.2}$ and $Y \sim I^{2.3\pm0.1}$ are the respective dependences for crystal and porous silicon.

Table 2. Maximum absolute yield of hard x-ray radiation Y in different energy intervals for different heating-radiation wavelengths and laser pulse lengths.

λ/nm	τ_1/ps	Filter	I_{max}/PW cm^{-2}	Y/nJ	K_x (10^{-6} %)	K_e (%)
1055	1	Be (200 μm)	8 ± 0.5	5.5 ± 0.5	65 ± 7	1.5 ± 0.3
527	1		10 ± 0.5	1.3 ± 0.2	36 ± 4	1.5 ± 0.3
351	1		7 ± 0.5	0.36 ± 0.05	25 ± 3	2.5 ± 0.5
1055	1	Be (200 μm) + Al (100 μm)	7 ± 0.5	4.5 ± 0.5	55 ± 5	3 ± 1
527	1		12 ± 0.5	0.9 ± 0.1	21 ± 2	3 ± 1
351	1		8 ± 0.5	0.1 ± 0.02	5.1 ± 0.5	3 ± 1
527	0.2		48 ± 5	0.05 ± 0.01	1.5 ± 0.2	0.2 ± 0.06

Note: K_x is the laser radiation-to-hard x-ray energy conversion coefficient; K_e is the laser radiation-to-electron beam energy conversion coefficient.

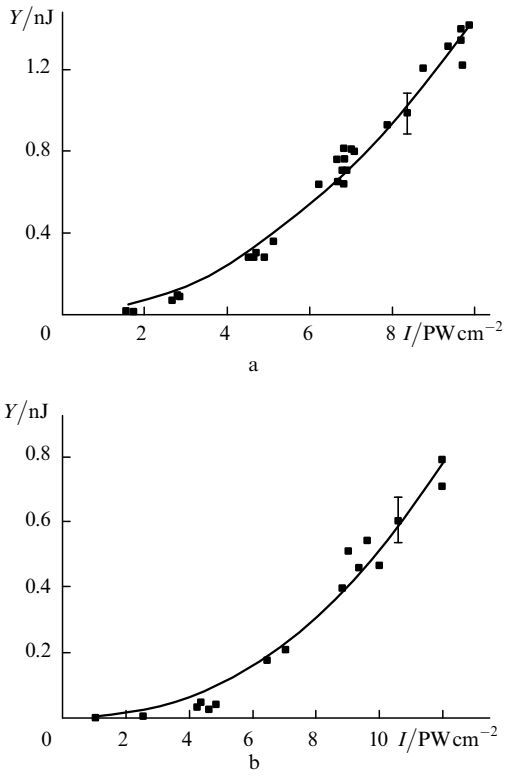

Figure 5. Hard x-ray radiation yield from the plasma of a crystal silicon target Y as a function of the laser radiation intensity I ($\lambda = 527$ nm, $\tau_1 = 1$ ps) for a beryllium filter 200 μm thick (a) and the filter combination Be (200 μm) + Al (100 μm) (b).

The results for crystal silicon agree well with the data obtained in our previous experiments involving irradiation by femtosecond pulses (200 fs in length, $\lambda = 600$ nm) with an energy contrast ratio of over 10^4 [1]. Volkov et al. [1] carried out measurements for comparable intensities by similar methods and using samples of crystal silicon and high-porosity silicon with the same degree of porosity as in the present work. The laser radiation-to-hard x-ray energy conversion coefficient measured in Ref. [6] was $\sim 10^{-6}$. The exponent of an approximating power function was in the range between 2.2 to 4.1, depending on the x-ray spectral range and the sample type. Gavrilov et al. [6] also noted that the hard x-ray yield was significantly higher when using a porous sample.

The intensity dependences of the hard x-ray yield in the $E > 9.8$ keV range for a laser pulse length of 200 fs and a poor (~ 20) energy contrast ratio (see Fig. 2b) exhibit an insignificant increase in the exponent from 2.2 ± 0.2 for a crystal silicon sample to 2.5 ± 0.2 for a high-porosity sample. However, this type of increase was not observed for the integral yield Y, which amounted to ~ 0.05 nJ for an intensity of the heating radiation of $\sim 5 \times 10^{16}$ W cm^{-2}. The laser radiation-to-hard x-ray conversion coefficient is $\sim 2 \times 10^{-8}$, which is an order of magnitude lower than that for a picosecond pulse.

Therefore, for pulse lengths of 1 and 0.2 ps, the distinctions between the dependences observed with crystal and porous silicon are insignificant in our experiments and are within the limits of experimental error. This fact may be attributed to structure homogenisation of the porous sample exposed to $\sim$ 1-ps-long pulses (or to a 200-fs-long pulse with a low contrast ratio), whereas it is precisely the porosity that should bring about an increase in the hard x-ray yield.

Indeed, the plasma expansion velocity exceeds 10^7 cm s^{-1} under the conditions realised in our experiments. Recognising that the cluster separation is ~ 10 nm, we conclude that the particles travel the 'intercluster' distance in 100 fs to smooth out the porous target structure. Conversely, the high contrast ratio of a femtosecond laser pulse in the experiments of Refs [2, 6] ensured interaction with a nonfuzzy nanostructured near-surface layer, which fprovided a more efficient generation of hot electrons and hard x-ray radiation.

The ratio between the signal in two channels with different filters can be used to estimate the temperature of hot electrons under the assumption that the electron velocity distribution is isotropic and Maxwellian [6, 7]. To this end, advantage was taken of the $Y(I)$ approximations for two filters obtained on a basis of experimental data. The result of processing the data shown above in Fig. 5 is given in Fig. 6. The approximating of the resultant dependence yields the relationship $T_h \sim I^{0.33 \pm 0.01}$ for the temperature of hot electrons. This lends support to the statement that the hot electron component is responsible for the production of the hard x-ray plasma radiation even for the 'moderate' intensities employed in our work.

As noted above, the hard x-ray radiation of a laser-produced plasma is indeed associated with the so-called hot electron component of the plasma. Collisions of hot electrons with ions give rise to bremsstrahlung or characteristic radiation of ions and atoms. Several mechanisms responsible for the generation of hot electrons are known at present. The prevalence of one or another mechanism is, to a large extent, determined by the intensity of laser radiation as well as by the ratio between the characteristic electron-density gradient scale length L (determined primarily by the plasma expansion in vacuum) and the wavelength of the heating radiation λ.

When advantage is taken of high-contrast (with a contrast ratio of over 10^5) $\sim$ 100-ps-long pulses with an intensity of $\sim 10^{17}$ W cm^{-2}, the above ratio is $L/\lambda \ll 1$. In this case, of greatest significance are the electron heating at the vacuum-plasma boundary [12, 13] and the heating due to the anomalous skin effect [14], when the temperature of hot electrons $T_h \sim (I\lambda^2)^{2/3}$. For picosecond pulses or femtosecond pulses with a poor contrast ratio, the electron density gradient is not that sharp and the absorption of laser radiation energy by the plasma is dominated by resonance absorption [15]. The resonance absorption is characterised by a power dependence

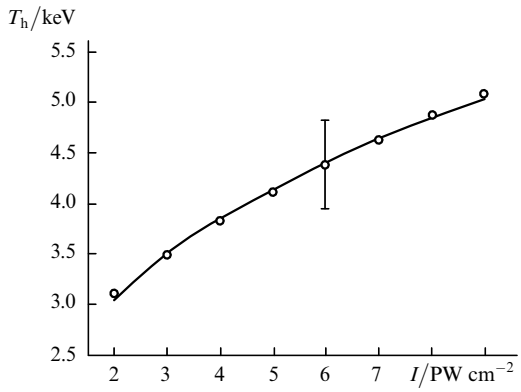

Figure 6. Temperature of hot electrons of the plasma of a crystal silicon target T_h as a function of the intensity of laser radiation I for $\lambda = 527$ nm (circles) and its approximation by a power function $T_h \sim I^{0.33}$ (the curve).

of the temperature of the hot electron component on the intensity I and the square of laser radiation wavelength λ with an exponent of 1/3 [16]:

$$T_h \approx 8\left(I\lambda^2\right)^{1/3}. \quad (1)$$

Here, the laser pulse intensity I is expressed in units of 10^{16} W cm^{-2}, the wavelength in micrometres, and T_h in kiloelectronvolts.

Therefore, the dependence obtained in our work is in good agreement with the theoretical predictions for the resonance mechanism of production of hot electrons.

4. Effect of wavelength of the heating radiation on the hard x-ray yield from the plasma

The wavelength dependence of the temperature of hot electrons was determined employing the experimental data on the hard x-ray radiation yield for different wavelengths ($\lambda = 1055$, 527, and 351 nm) for a laser pulse length of 1 ps. Five different filters (Fig. 4) were used to record the hard x-ray spectrum. The temperature T_h of hot electrons was estimated for different filter combinations.

Fig. 7 gives the dependence obtained for the temperature T_h. Th is approximated by the function $T_h \approx (5.2\pm\ 0.3)$ $(I\lambda^2)^{0.34\pm0.03}$, which is consistent with theoretical conceptions. An insignificant difference in the absolute temperature values (the factor 5.2 in lieu of 8) may be due to the inadequacy of introducing the notion 'temperature' for the non-thermal fraction of the electron plasma component. Moreover, there is a systematic error of the 'temperature' evaluation technique in use, which implies a strictly exponential shape of the tail of the x-ray photon spectral distribution. On the other hand, relationship (1) is also approximate, for it was found in numerical simulations and not analytically.

Based on the data on the dependence of the hot-electron temperature and the hard x-ray radiation yield from the plasma on the wavelength of a laser pulse, it is possible to estimate the energy absorbed by the hot electron component. The energy of electron beam bremsstrahlung in the filter transmission band $F(E)$ can be estimated by resorting to the simple formula [7]

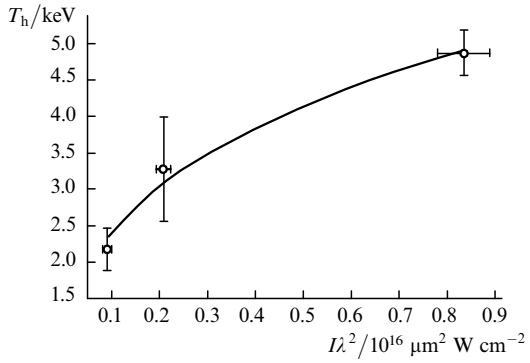

Figure 7. Temperature of hot electrons in the plasma of a crystal silicon target T_h as a function of the laser radiation intensity I and wavelength λ (circles) and its approximation by a power function $T_h \sim (I\lambda^2)^{0.34}$ (the curve).

$$E_x \approx K_e W \int_0^\infty F(E)e^{-E/T_h}dE \Big/ 10^{-6} Z T_h,$$

where K_e is the sought-for coefficient of conversion of the laser pulse energy W to the energy of hot electrons; Z is the atomic number of the radiating atoms. The result of our data processing is given in the last column of Table 2.

5. Conclusions

Therefore, resonance absorption is the chief mechanism of generation of the hot electron component in a plasma produced by picosecond laser pulses.

We have for the first time measured in a single experiment the dependence of the hard x-ray yield from a plasma produced by ultrashort laser pulses on the wavelength and the intensity of laser radiation. The dependences of the 'temperature' of the hot electron component on the intensity and the wavelength of laser radiation, which were derived from our experimental data, are consistent with the theoretical conceptions of the resonance mechanism of absorption of the laser radiation.

The length of a laser pulse and its contrast ratio have a strong effect on the nature of interaction and the processes in the plasma in the case of nanostructured targets. In particular, the target structuring ceases to affect on the form of the dependences and the absolute yield of hard x-ray radiation in the case of 200-fs pulses with a low contrast ratio and 1-ps pulses.

The TWINKLE laser system can be validly used to implement an efficient source of hard x-ray radiation with a pulse length of ~ 1 ps. The measured coefficient of conversion to the $E > 2.5$ keV hard x-ray photon energy range amounts to $\sim 6.5 \times 10^{-5}$% for an absolute yield of 5.5 nJ, with approximately 2% of the laser pulse energy going into the hot electron component. The high pulse repetition rate of the TWINKLE system, which may be as high as 30 Hz, may also prove to be beneficial to many applications where picosecond x-ray diagnostics of materials is involved.

Acknowledgements. The authors express their gratitude to R Danelyus and P M Mikheev for their fruitful discussions concerning the issues addressed in this paper. This work was supported by the Russian Foundation for Basic Research (Project No. 99-02-18343), the 'Russian Universities' and 'Fundamental Metrology' State Scientific-Technical Programmes, and the State Foundation of Lithuania for Science and Education (Contract No. KA-016/reg. 98823).

References

1. Volkov R V, Gordienko V M, Dzhidzhoev M S, et al. Kvantovaya Elektron. (Moscow) **24** 1114 (1997) [Quantum Electron. **27** 1081 (1997)]
2. Volkov R V, Gordienko V M, Dzhidzhoev M S, et al. Kvantovaya Elektron. (Moscow) **25** 3 (1998) [Quantum Electron. **28** 1 (1998)]
3. Stuart B C, Perry M D, Miller J, et al. Opt. Lett. **22** 242 (1997)
4. Beg F N, Bell A R, Dangor A E Phys. Plasmas **4** 447 (1997)
5. Gordienko V M, Savel'ev A B Usp. Fiz. Nauk **169** 78 (1999) [Phys. Usp. **42** 72 (1999)]
6. Gavrilov S A, Golishnikov D M, Gordienko V M, et al. Proc. SPIE Int. Soc. Opt. Eng. **4070** (2000)
7. Schnurer M, Kalashnikov M P, Nickles P V, et al. Phys. Plasmas **2** 3106 (1995)
8. Saemann A, Eidmann K Appl. Phys. Lett. **73** 1334 (1998)
9. Yu J, Jiang Z, Kieffer J C, Krol A Phys. Plasmas **6** 1318 (1999)

10. Wang Y, Luther-Davies B Opt. Lett. **17** 1459 (1992)
11. Stabinis A, Valiulis G, Ibragimov E A Opt. Commun. **86** 301 (1991)
12. Brunel F Phys. Rev. Lett. **59** 52 (1987)
13. Gibbon P, Bell A R Phys. Rev. Lett. **68** 1535 (1992)
14. Andreev A A, Gamalii E G, Novikov V N Zh. Eksp. Teor. Fiz. **101** 1808 (1992) [Sov. Phys. JETP **74** 963 (1992)]
15. Meyerhofer D D, Chen H, Delettrez J A, et al. Phys. Fluids B **5** 2584 (1993)
16. Gibbon P, Forster E Plasma Phys. Controlled Fusion **38** 769 (1996)